Journal of Colloid and Interface Science 578 (2020) 242–253

Contents lists available at ScienceDirect

Journal of Colloid and Interface Science

journal homepage: www.elsevier.com/locate/jcis

Micro- and macroscopically structured zwitterionic polymers with ultralow fouling property

Dong Zhang [a], Baiping Ren [a], Yanxian Zhang [a], Yonglan Liu [a], Hong Chen [a], Shengwei Xiao [b], Yung Chang [c], Jintao Yang [d], Jie Zheng [a,*]

[a] Department of Chemical, Biomolecular, and Corrosion Engineering, The University of Akron, OH 44325, USA
[b] School of Pharmaceutical and Materials Engineering, Taizhou University, Taizhou 318000, China
[c] Department of Chemical Engineering and R&D Center for Membrane Technology, Chung Yuan Christian University, Taoyuan 320, Taiwan
[d] College of Materials Science& Engineering, Zhejiang University of Technology, Hangzhou, 310014, China

GRAPHICAL ABSTRACT

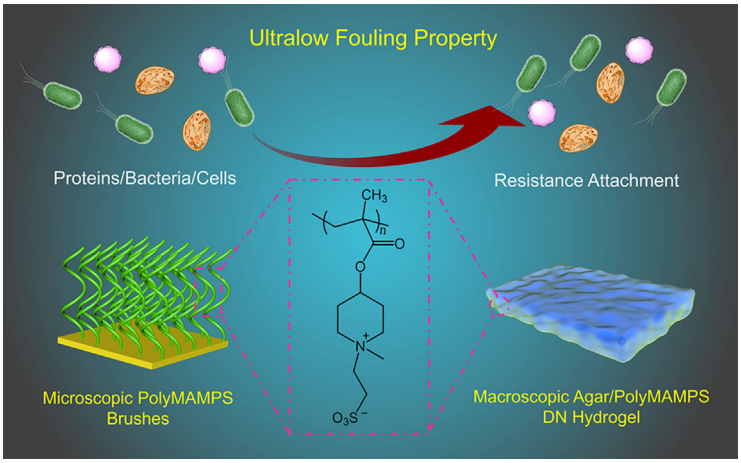

ARTICLE INFO

Article history:
Received 12 March 2020
Revised 29 April 2020
Accepted 31 May 2020
Available online 3 June 2020

Keywords:
Antifouling
Polyzwitterionic materials

ABSTRACT

Hypothesis: Polyzwitterions as a promising class of materials are often used to construct antifouling surfaces with optimized conformation and compositions for a wide variety of antifouling applications. While numerous zwitterionic polymers have been identified for their antifouling capacity, the exact relationship among molecular structure, surface hydration property, and antifouling performance of zwitterionic polymers at different scales still remains elusive.
Experiments: we first designed and synthesized a new zwitterionic monomer of *3-(4-(methacryloyloxy)-1-methylpiperidin-1-ium-1-yl)-propane-1-sulfonate* (MAMPS), then used MAMPS monomers to fabricate into homogenous polymer brushes on Au substrate using SI-ATRP and heterogeneous double-network (DN) hydrogels combining with Agar network via one-pot, heating-cooling-photopolymerization method,

Abbreviations: MAMPS, 3-(4-(methacryloyloxy)-1-methylpiperidin-1-ium-1-yl)propane-1-sulfonate; DN, double-network; SN, single-network; SI-ATRP, surface-initiated atom transfer radical polymerization; TCPS, tissue culture polystyrene. polySBMA, poly(sulfobetaine methacrylate); polyCBMA, poly(carboxybetaine methacrylate); polyVBIPS, poly(3-(1-(4-vinylbenzyl)-1H-imidazol-3-ium-3-yl)propane-1-sulfonate); polyDVBAPS, poly(3-(dimethyl(4-vinylbenzyl) ammonio) propyl sulfonate); polySVBP, poly(2-(1-(4-vinylbenzyl)pyridin-1-ium-4-yl)ethane-1-sulfonate); MA-PD, 1-methylpiperidin-4-yl methacrylate; SPR, surface plasma resonance; SAM, self-assembled monolayer; AFM, Atomic Force Microscopy; BAEC, Bovine aortic endothelial cells; Fg, fibrinogen; ELISA, enzyme-linked immunosorbent assay; FT-IR, Fourier-transform infrared spectroscopic; polyMPC, poly(2-methacryloyloxyethyl phosphorylcholine); MBAA, N, N'-methylenebisacrylamide.

* Corresponding author.
E-mail address: zhengj@uakron.edu (J. Zheng).

https://doi.org/10.1016/j.jcis.2020.05.122

Polymer brush
Double-network hydrogel

and finally evaluated their antifouling ability to resist the adsorption of protein/cell/bacteria on the two different polymer forms at microscopic and macroscopic scales.
Findings: For microscopic polyMAMPS brushes, they exhibited excellent resistance to nonspecific protein adsorption from both undiluted blood serum/plasma (0.3–5 ng/cm^2), cell adhesion up to 3 days, and clinically relevant bacterial attachment for 72 h at the optimal film thicknesses of 20–40 nm. For macroscopic Agar/polyMAMPS DN hydrogels, they also exhibited approximately 96% less protein adhesion than tissue culture polystyrene (TCPS). Different structured materials consisting of polyMAMPS at both micro- and macro-scales demonstrate its excellent, intrinsic antifouling property, which could be related to their highly water binding character of zwitterionic groups. PolyMAMPS materials, alternative to commonly used poly(sulfobetaine methacrylate) (polySBMA) and poly(carboxybetaine methacrylate) (polyCBMA) zwitterions, hold great promise for antifouling designs and applications.

1. Introduction

Antifouling materials and coatings have been demonstrated as their desirable functions and properties for many industrial and biomedical applications, including implanted devices [1–3], drug/-gene delivery carriers [4,5], marine coatings [6–9], and wastewater membranes [10–12]. Biofouling is a long-standing, unsolved problem, in which a wide variety of biofoulants (e.g. proteins, cells, bacteria, pathogen, and fungus) are easily adsorbed on many different artificial substrates (e.g. organic, inorganic, and biological substances) via different fouling mechanisms [13,14]. Among different fouling mechanisms, they almost all involve the initial adsorption of non-specific proteins on substrates, which will further initiate and facilitate primary micro-colony growth, secondary irreversible attachment, and final biofilm formation [12,15]. For instance, even ~5 ng/cm^2 of fibrinogen adsorption on the surgical implants triggers the complex foreign body response and immune rejection [16,17]. Thus, the early prevention of non-specific protein adsorption is considered as the most promising strategy against biofilm formation.

Engineering interfaces by polymers or other materials in aqueous systems have a large and direct influence on water dynamics and structures near the interfaces at a nano-scale, which in turn affect the subsequent water-involved processes [18]. Currently, antifouling polymers can be generally grouped into four typical types of polyethylene glycol (PEG) [19], polyacrylates [20], polysaccharides [21], polyamides [22], and polyzwitterions [23] based on their hydrophilic and charge characteristics. In general, "grafting-to" (e.g., spinning coating, physical or chemical adsorption, dip-coating, electrospinning, and physical vapor deposition) and "grafting-from" (e.g., atom transfer radical polymerization, reversible addition-fragmentation chain transfer polymerization) strategies are often used to coat antifouling polymers onto the substrates to create antifouling surfaces with well controlled chain morphology, surface topology, and grafting density [21,24]. The resultant surfaces coated by both hydrophilic and zwitterionic polymers achieve their antifouling property by forming a strong surface hydration barrier to resist foulant adsorption. The antifouling performance of these antifouling surfaces is determined by intrinsic physicochemical property of polymers themselves (e.g., hydrophilicity, charge distribution/density, pendant groups, carbon space length) and the extrinsic surface topologies (e.g., surface hydrophilicity, roughness, thickness, grafting density). Different from passive antifouling strategies (e.g. foulant repelling and surface coating micropatterns) that use intrinsic antifouling properties of materials and surfaces alone to prevent the general adsorption of foulants on the surfaces without killing or damaging foulants, active antifouling strategies including contact inhibition of foulants [25], contact killing/release of foulants [26–29], catalytic degradation and enzymatic reactions [30,31], and different nontoxic inhibitors to block cell/bacteria communications [32] aim to use chemical compounds to interfere with the bioactivity of foulants by killing them and inhibiting their surface adhesion, proliferation, and communication capacity [12]. While both strategies have their own merits, a combination of both passive and active antifouling strategies is more promising to increase antifouling performance in a complement or synergistic way for real-world applications.

We have previously used surface-initiated atom transfer radical polymerization (SI-ATRP) to prepare a series of hydrophilic polyamide and polyacrylate brushes, all of which exhibited high surface resistance to protein adsorption from undiluted blood serum/-plasma, cell adhesion, and bacterial colony at superlow or nonfouling level [33–37]. Different from these hydrophilic-based polymer brushes, zwitterionic polymers possess a combination of the equal number of cationic groups (e.g. phosphonium, pyridinium, imidazolium and quaternary/tertiary/secondary/primary ammonium groups) and anionic groups (e.g. carboxylate, sulfonate, and phosphate groups) in the same pendant motif [38,39]. Such unique structural feature also empowers zwitterionic polymers to have strong electrostatically-induced interactions with water molecules via ionic solvation [40]. The unique hydration properties of zwitterionic polymers have been well recognized and used for antifouling materials and surfaces. Poly(sulfobetaine methacrylate) (polySBMA), poly(carboxybetaine methacrylate) (polyCBMA), phosphobetaine-based zwitterionic materials have dominated research efforts and demonstrated their antifouling properties for longer circulation times of biomedical implanted devices in blood, wound regeneration, and biological tissues [41–44]. Among them, sulfobetaine-based polyzwitterions have relatively more derivatives due to the higher reaction yield and the cheap prices, including poly(3-(1-(4-vinylbenzyl)-1H-imidazol-3-ium-3-yl)propane-1-sulfonate) (polyVBIPS), poly(3-(dimethyl(4-vinylbenzyl) ammonio) propyl sulfonate) (polyDVBAPS), and poly(2-(1-(4-vinyl benzyl)pyridin-1-ium-4-yl)ethane-1-sulfonate) (polySVBP), all of which achieve strong antifouling property via salt-induced anti-polyelectrolyte effect [26,45–48], i.e. polymer chains adopt collapsed conformations in water while stretched conformations in salt solutions. However, it still remains a great challenge to design new zwitterionic structures, moieties, and materials due to very limited availability of anionic groups [49].

To increase the structural diversity of zwitterionic polymers, herein we first designed and synthesized a new zwitterionic monomer of *3-(4-(methacryloyloxy)-1-methylpiperidin-1-ium-1-yl)-propane-1-sulfonate* (MAMPS), then used MAMPS monomers to fabricate into homogenous polymer brushes on Au substrate using SI-ATRP and heterogeneous double-network (DN) hydrogels combining with Agar network via one-pot, heating-cooling-photopolymerization method, and finally evaluated their antifouling performance on the two different polymer forms at microscopic and macroscopic scales (Fig. 1). For microscopic polyMAMPS brushes, given the optimal film thicknesses of 20–40 nm and high grafting

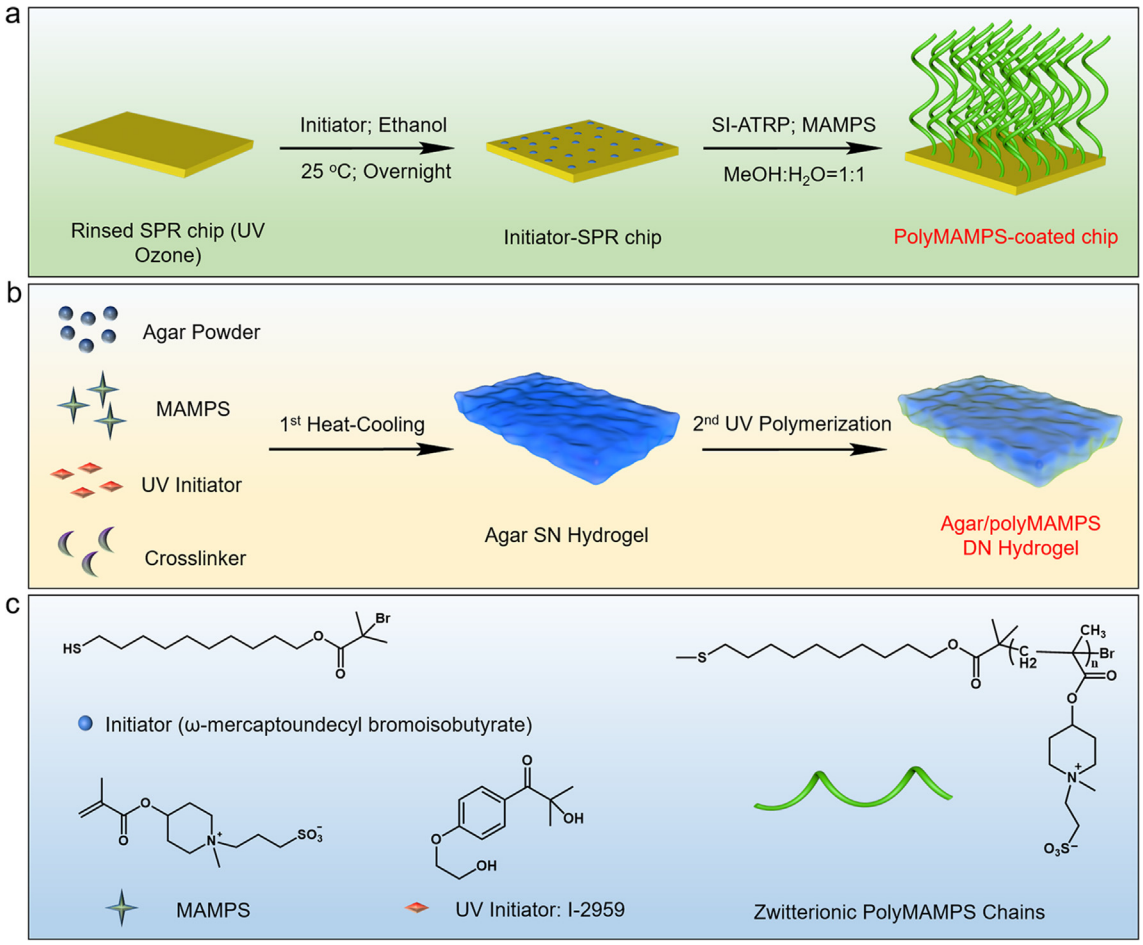

Fig. 1. Design and synthesis of microscopic polyMAMPS brushes and macroscopic Agar/polyMAMPS double-network hydrogel. (a) General SI-ATRP process of grafting polyMAMPS on a SPR chip surface coated with immobilized initiator. (b) "One-pot" synthesis procedure of Agar/polyMAMPS DN hydrogel via typical heating-cooling-UV polymerization. (c) Chemical structures of MAMPS monomer, polyMAMPS chain, UV initiator for polyMAMPS SN and Agar/polyMAMPS DN hydrogels, and initiator for SI-ATRP method.

density, polyMAMPS brushes realized high surface resistance to nonspecific protein adsorption (0.3–5 ng·cm^{-2}) from undiluted blood serum and plasma, cell adhesion, and bacterial colony. Different from polymer brush as an ideal model system making it impractical for real applications, hydrogels are an important class of practical biomaterials for a wide variety of real applications. For macroscopic Agar/polyMAMPS DN hydrogels, this hydrogel system significantly improved not only mechanical tensile properties from 0.16 MPa at 35% strain to 0.21 MPa at 145% strain, but also antifouling property against cell adhesion, as compared to Agar single-network hydrogel. Similar to other zwitterionic polymers, strong surface hydration of polyMAMPS occurs due to the formation of ionic solvation around zwitterionic groups. This work demonstrates a new zwitterionic polyMAMPS system that can be generally applied to both microscopic and macroscopic polymer forms while retaining the same antifouling activity, and offers some insights into the fundamental structure-function relationship among zwitterionic polymer, surface hydration, and antifouling performance, which hopefully will guide the structural-based design of new zwitterionic materials.

2. Materials and methods

2.1. Materials

ω-mercaptoundecyl bromoisobutyrate, as a small molecule initiator, was synthesized by our previous work [37]. 1-methyl-4-piperidino, methacryloyl chloride, triethylamine, anhydrous CH_2Cl_2, 1, 3-propanesultone, human plasma fibrinogen (Fg), bovine serum albumin (BSA), phosphate buffer saline (PBS), γ-butyrolactone, trifluoroethanol, Me_6TREN, CuBr, methanol, N, N'-methylenebisacrylamide, Agar, anhydrous acetone, and hydrochloric acid (HCl) were purchased from Sigma-Aldrich Co., Ltd. Anhydrous sodium sulfate, o-phenylenediamine, and anhydrous acetone were purchased from TCI Co., Ltd. Horseradish peroxidase (HRP)-conjugated polyclonal goat antihuman fibrinogen was purchased from US Biological. Water was purified by a Millipore water purification system with a minimum resistivity of 18.0 MΩ cm. All other chemicals or biological culture were used as received without any purification.

2.2. Synthesis of MA-PD and zwitterionic monomer MAMPS

1-methylpiperidin-4-yl methacrylate (MA-PD) was synthesized by the reaction of methacryloyl chloride and 1-methyl-4-piperidino. Specifically, methacryloyl chloride (0.058 mol, 6.062 g) in 50 mL of anhydrous CH_2Cl_2 was added dropwise to the solution of 1-methyl-4-piperidino (0.05 mol, 5.769 g) and triethylamine (0.108 mol, 15 mL) dissolved in 50 mL anhydrous CH_2Cl_2 at 0 °C ice bath (high purity nitrogen environment). The mixture was stirred for 3 h and then heated up to 25 °C for an additional 12 h. After the reaction, 80 mL pure water was poured into reactor to remove the unreacted methacryloyl chloride. The organic layer was washed with 10% ammonia solution, pure water

twice, separated by separatory funnel and dried by anhydrous sodium sulfate overnight. Finally, the organic solution was concentrated, evaporated to dryness under reduced pressure. The yield of the purified liquid product MA-PD (*1-methylpiperidin-4-yl methacrylate*) is 52%. Product identity and purity were confirmed by ^{1}H NMR (300 MHz, DMSO d_6): (ppm), 2.05–2.15 (3H), 6.00–6.20 (2H), 5.0–5.05 (1H), 1.85–1.95 (4H), 2.65–2.75 (4H), and 3.00–3.20 (3H).

3-(4-(methacryloyloxy)-1-methylpiperidin-1-ium-1-yl)-propane-1-sulfonate (MAMPS) was synthesized according to the ring-opening reaction using 1, 3-propanesultone and MA-PD. Under an anhydrous condition, 6.00 g (0.033 mol) MA-PD and 4.00 g (0.033 mol) 1, 3-propanesultone were dissolved with 10 mL anhydrous acetone in a 50 mL round-bottom flask. Control reaction time of 48 h and reaction temperature of 30 °C, the zwitterionic product MAMPS can obtained under reducing pressure. After complete dry under reduced pressure, the yield of purified monomer MAMPS is 62%. Product identity and purity were confirmed by ^{1}H NMR (300 MHz, DMSO d_6): (ppm), 1.98–2.03 (3H), 5.92–6.20 (2H), 4.44–4.50 (1H), 1.85–1.95 (2H), 3.65–3.70 (4H), 3.30–3.40 (7H), 2.65–2.75 (2H), and 1.20–1.40 (2H).

2.3. PolyMAMPS brushes on SPR chip

SPR (surface plasma resonance) chip was rinsed with ethanol, acetone and water sequentially, later treated under UV ozone for 20 min, washed by DI-water and finally air-dried. Before surface initiated (SI)-ATRP, an initiator self-assembled monolayer (SAM) was first anchored onto the SPR chips by soaking SPR chips into 1 mM ω-mercaptoundecyl bromoisobutyrate (initiator) ethanol solution at room temperature overnight due to the unique strong interaction between sulfhydryl group and Au atoms. Furthermore, the chip was washed with ethanol and air-dried before live polymerization process. Fig. 1a showed an essential process of grafting polyMAMPS brushes onto the initiator-SPR chip surface via SI-ATRP method. SI-ATRP enabled to establish a desirable atomic scale precision in surface topology and chemistry. Briefly, under the protection of nitrogen, one tube containing MAMPS (1.80 g), Me_6TREN (60 mg), and degassed methanol:water (1:1, v%) solution were transferred to the second tube containing SPR gold chip coated with immobilized initiators and CuBr (12.5 mg) and then SI-ATRP reaction was immediately started at room temperature. After the controlled reaction time, the reaction was stopped by exposing to air. In order to remove unreacted monomers or unbounded polymer, the chips were soaked in PBS buffer overnight. Here, we used four reaction solvents to optimize the polymerization process, including methanol: H_2O (1:1, v%), trifluoroethanol: H_2O (1:1, v%), trifluoroethanol: ethanol (1:1, v %), and methanol: ethanol (1:1, v%) solutions. Polymer brushes with various thicknesses were simply controlled by tuning the polymerization time, mainly from 0 to 24 h.

2.4. Synthesis of Agar/polyMAMPS double-network hydrogel

Macroscopic Agar/polyMAMPS DN hydrogels were synthesized by the typical heating–cooling-UV polymerization method. In brief, a glass tube containing MAMPS (2.0 g), Agar (0.15 g), initiator I-2959 (7.35 mg), and (with or without) crosslinker MBAA (1.01 mg) was mixed with 5 mL degassed water. To form a transparent precursor solution, the tube was the sealed under high purity nitrogen protection and heated up to 95 °C to dissolve Agar in a water bath. Thereafter, the transparent precursor was immediately injected into a glass mold (1 mm thickness) and gradually cooled down to room temperature. Once the first physical polysaccharide network formed, the mold was exposed to the UV light (365 nm) for ~2 h, to fully generate chemical-crosslinked second polyMAMPS network (Fig. 1b).

2.5. Brush thickness of polyMAMPS brushes by ellipsometry

The thickness of polyMAMPS brushes was measured by a multiple wavelength mode ellipsometer (J.A. Woollam Co. Ltd.) with a wavelength range of 400–800 nm at a fixed incident angle. In order to reduce instrument errors, a special Cauchy model were chosen to fit curve for bare SPR surface and then to read the brush thickness simultaneously. The average thickness were determined by measuring three different locations of each sample.

2.6. Hydrophilicity of polyMAMPS brushes by water contact angle

Water contact angle of polyMAMPS brush surface was measured by a sessile drop technique on a RameHart goniometer (Mountain Lake, NJ), using Millipore water under ambient conditions. The average water contact angles were determined by measuring three different locations of each sample.

2.7. Surface morphologies by atomic Force microscopy (AFM)

Surface morphology and roughness of polyMAMPS brushes were examined by Nanoscope IIId AFM in a tapping mode (Veeco Inc.). PolyMAMPS brushes with different thicknesses were scanned at a typical rate of 1.0–2.0 Hz with a vertical tip oscillation frequency of 170–180 kHz. Both 2D and 3D images were acquired by detectors.

2.8. Protein adsorption by SPR measurement

A customized SPR sensor based on wavelength interrogation was used to determine protein adsorption performance on polyMAMPS brushes of different thicknesses. The solution (undiluted human protein solution or PBS buffer) was flowed through 4 channels under the pressure of peristaltic pump. Firstly, the SPR chip coated with polyMAMPS brushes were connected to the surface of prism. A normal baseline signal was measured by flowing PBS solution through the detector of sensor. Each protein solution, i.e. 100% human blood plasma or serum, was independently flowed through channels for ~10 min, and SPR wavelength would shift if any protein adsorption happened. Usually, due to the nonspecific adhesion of the protein, the wavelength pattern would generate an ascending "step". After that, the protein solution was replaced by PBS solution again to remove the unbound or slightly bounded protein on the prism surface and maintained > 10 min. The flow rate of solutions were controlled at 0.05 mL·min^{-1}. The wavelength shift, mainly derives from the difference value between the PBS baselines obtained before and after corresponding protein solution flow. It should be pointed out that a 1 nm SPR wavelength shift at 750 nm corresponds to ~15 ng·cm^{-2} protein adsorption.

2.9. Cell adhesion

Bovine aortic endothelial cells (BAEC) were chosen to challenge the surface of the polyMAMPS brushes. Just as mentioned in previous work, BAEC cell lines were firstly culture in the special-made medium on a tissue culture polystyrene flask for ~72 h to reach a high density. Then, BAEC were removed from the flask by the reported protocol and diluted to a concentration of 10^5 cells·mL^{-1}. Before coculture experiment, the samples needed sufficient sterilization and immerse into sterile PBS buffer for 24 h. Then a diluted 3 mL cell suspension was added to each corresponding well after samples were placed into a six-well flask. The incubated temperature was controlled at 37 °C for another 72 h. Cell morphology

were determined by an EVOS XL core inverted microscope with a 10× objective.

2.10. Bacteria attachment

Two typical bacteria (*E. coli*, Gram-negative and *S. epidermidis*, Gram-positive) were chosen for the bacterial attachment measurement. In brief, several colonies of each bacteria were firstly chosen and incubated in moderate LB medium to get the initial bacterial culture solutions. Then the initial bacterial solution were diluted to achieve a final density of 10^5 cells/cm^2. A diluted 4 mL bacterial suspension was added to each well after sterilized chips grafted with polyMAMPS brushes of various thicknesses and different bulk hydrogels were placed into a six-well flask. The whole systems were incubated under the room temperature for ~12 h. After 12 h, the samples were washed with Mili-Q water twice, and stained with a Live/Dead BacLight kit (Thermo Fisher Scientific Inc., NY) before imaging. The morphology of sample was measured by the Olympus IX81 fluorescence microscope with a 40× lens.

2.11. Fibrinogen adsorption onto macroscopic hydrogels by ELISA

The adsorption of fibrinogen (Fg) onto bulk hydrogels was measured by using the standard ELISA (enzyme-linked immunosorbent assay) process, as reported previously. Generally, all as-prepared hydrogel samples were immersed into PBS at room temperature for at least ~72 h to remove unreacted monomer and reach swelling equilibrium. Then the hydrogels were cut into 8 mm circular disks and placed into individual wells of a 24-well plate. Then the hydrogels were successively incubated with 250 μL Fg solution in PBS for 90 min (1 mg·mL^{-1}), 250 μL BSA solution in PBS (1 mg·mL^{-1}) for 90 min and 250 μL of HRP-anti-Fg solution in PBS (10 μg·mL^{-1}) for 30 min at 37 °C. For each change of the incubated solution, the samples needed to rinse with pure PBS buffer five times. During the dyeing process, the gel disks were transferred into a new well, and 250 μL of citrate phosphate buffer (0.1 M, pH = 5.0) containing 1 mg·mL^{-1} o-phenylenediamine and 0.03% hydrogen peroxide was injected into each well and maintained for 20 min. Enzyme activity finally stopped by adding an equal volume of 250 μL of 1 M HCl solution to each well. The light absorbance of the supernatant was measured at 492 nm by using a microplate reader (Infinite M200), and the surface of tissue culture polystyrene (TCPS) was used as a control for reference.

2.12. FT-IR spectral analysis

Fourier-transform infrared spectroscopic (FT-IR) analysis was recorded by using a Thermo Nicolet (Nicolet 6700) with resolution at 4 cm^{-1} and scans at 32, which completely evaluated chemical structures of lyophilized Agar SN and Agar/polyMAMPS DN hydrogels.

3. Results and discussion

3.1. Synthesis and characterization of polyMAMPS brushes

Fig. 2a showed a synthesis route for a hexacyclic zwitterionic monomer of *3-(4-(methacryloyloxy)-1-methylpiperidin-1-ium-1-yl) propane-1-sulfonate* (MAMPS). Briefly, methacryloyl chloride was added dropwise to the mixture of 1-methyl-4-piperidino, triethylamine, and anhydrous CH_2Cl_2 at 0 °C ice bath under nitrogen protection for synthesizing intermediate *1-methylpiperidin-4-yl methacrylate* (MA-PD). Then, MA-PD was reacted with 1, 3-propanesultone to produce *3-(4-(methacryloyloxy)-1-methylpiperidin-1-ium-1-yl)-propane-1-sulfonate* (MAMPS) via a ring-opening reaction, with a yield rate of purified MAMPS monomer of ~62%. ^{1}H NMR spectra in Fig. 2b-c showed the characteristic chemical peaks of intermediate product of MA-PD and final product of MAMPS. The chemical shifts in the range of 6.00–6.20 ppm were attributed to hydrogen protons of CH_2=C group in MA-PD, whi-

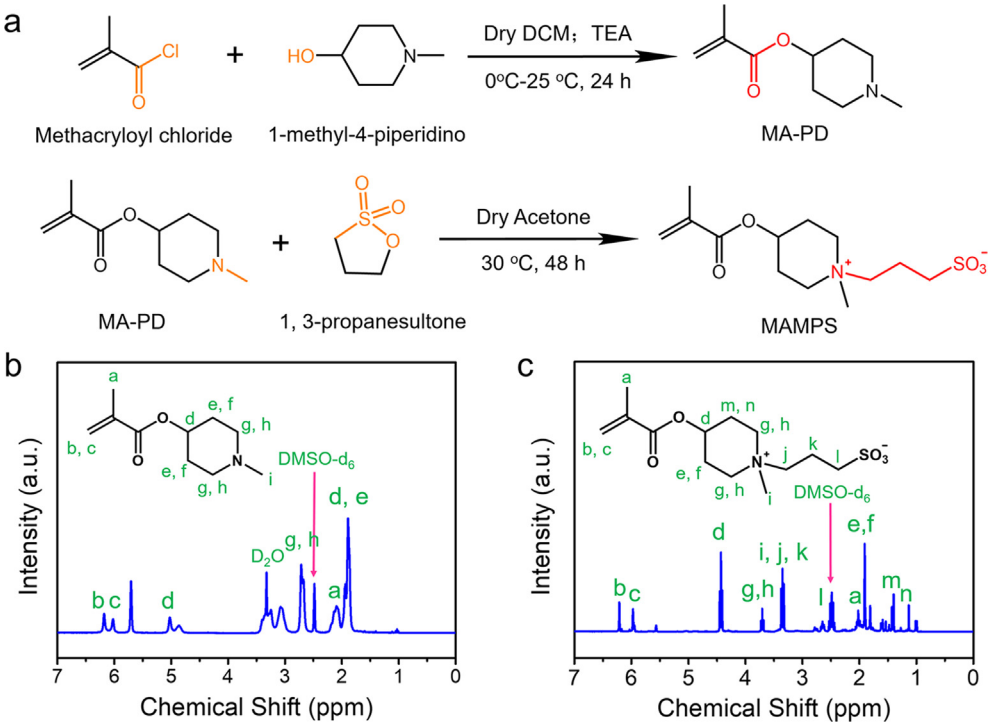

Fig. 2. (a) Synthesis procedure of intermediate MA-PD monomer and final MAMPS monomer. ^{1}H NMR spectrum of (b) MA-PD and (b) MAMPS monomers (300 MHz, DMSO d_6).

le the chemical shifts at 3.30–3.40 ppm and 6.00–6.20 ppm were associated with hydrogen protons from alkane group between sulfonic group and quaternary ammonium groups as well as CH_2=C group in MAMPS, indicating the successful integration of 1, 3 propane sultone into vinyl monomer backbone via ring-opening polymerization.

Upon obtaining MAMPS monomer, we further grafted and polymerized MAMPS monomers on Au chips to form polyMAMPS brushes with different thicknesses using the SI-ATRP method. A number of studies have reported that apart from polymer chemistry itself (e.g. hydrophilicity, charge types and distribution, pendant groups), surface morphology (e.g. surface roughness and film thickness) of polymer brushes also play an important role in antifouling performance[22,34,50–52]. Here, we proposed and demonstrated two different strategies to control the brush thickness of polyMAMPS brushes by changing reaction times and solvents during the SI-ATRP process. As shown in Fig. 3a, brush thickness increased almost linearly from ~8 nm to ~90 nm as reaction times from 6 h to 24 h. In addition, use of different solvents of methanol:water (1:1 v%), trifluoroethanol:water (1:1 v%), trifluoroethanol:ethanol (1:1 v%), and methanol:ethanol (1:1 v%) can achieve ~30 nm, ~35 nm, ~7 nm, and ~5 nm brush thickness after 12 h reaction, respectively (Fig. S1). Unless mentioned otherwise, we used the methanol: water solvent to prepare polyMAMPS brushes and characterize their surface morphology-antifouling property relationship.

To characterize the surface hydrophilicity of the sequential coatings from bare Au surface to polyMAMPS brush, Fig. 3b showed the dynamic change of water contact angles on bare Au chip, initiator-chip, and polyMAMPS-coated chip surfaces. It can be seen that upon coating with hydrophobic brominated initiators on Au chip, contact angles increased from ~53° to ~76.5°. However, after grafting of ~25 nm polyMAMPS chains above brominated initiators, contact angle immediately dropped to 32°, which was another indicator of the successful coating of polyMAMPS brush on Au surface. Furthermore, we examined the effect of brush thickness on water contact angles. As shown in Fig. 3c, when brush thickness was less than 10 nm, polyMAMPS exhibited a larger water contact angle of ~64° and did not present high surface wettability. As brush thickness was increased to ~10 nm, water contact angle dropped immediately to ~44°. Further increase of brush thickness to a range of 12–40 nm did not largely alter water contact angle of ~32°. Since a zwitterionic MAMPS group as a building block is a typical hydrophilic group, increase of brush thickness leads to an increase of MAMPS groups and thus surface hydrophilicity reaches to a saturated value.

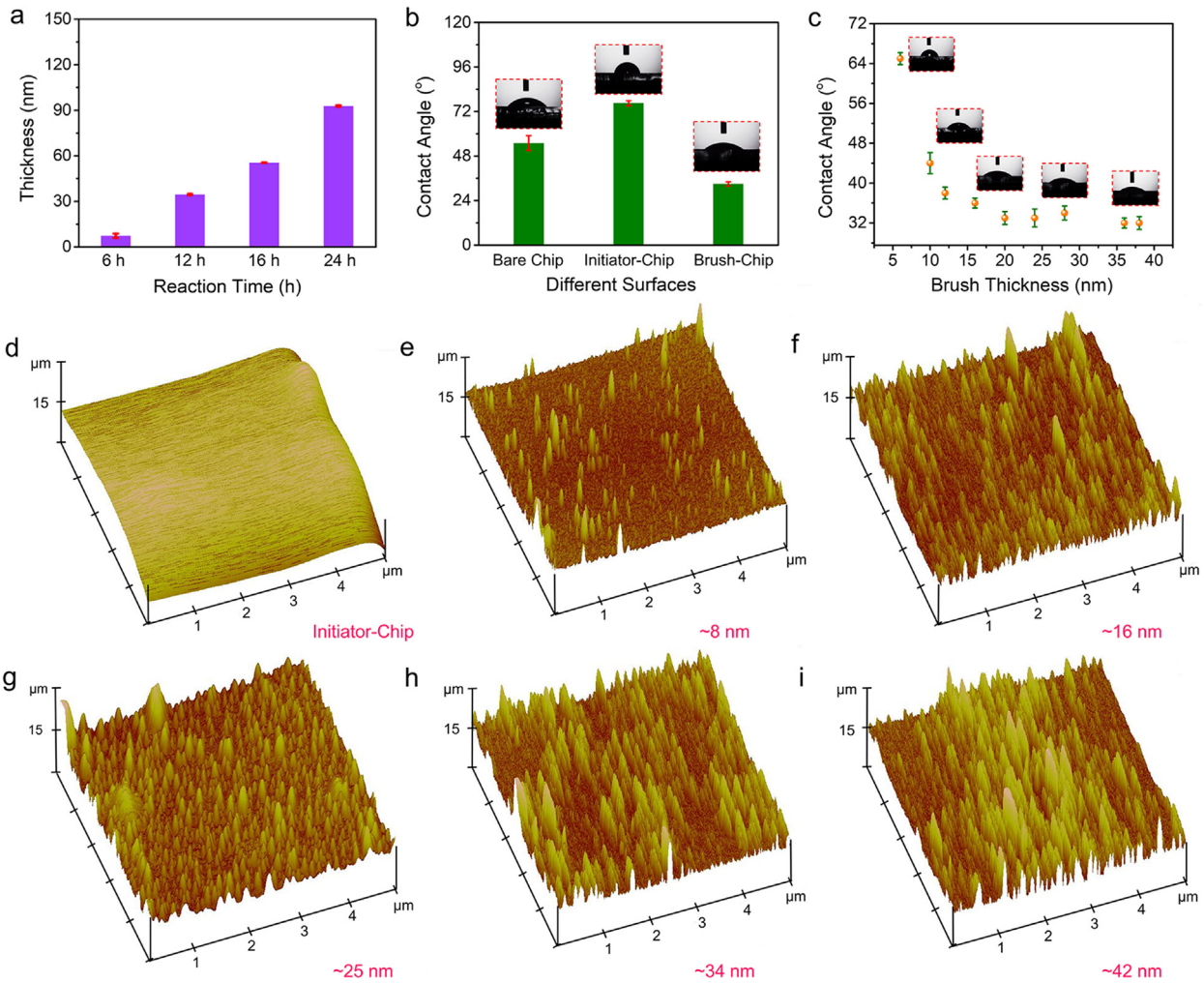

Fig. 3. Surface characteristics of polyMAMPS brushes. (a) Thickness of polyMAMPS brushes as a function of SI-ATRP reaction time. (b) Water contact angles for bare Au, initiator-coated, and polyMAMPS brush-coated (~25 nm) surfaces. (c) Dependence of water contact angle on the thickness of polyMAMPS brushes. 3D Tapping-mode AFM images for (d) initiator- and polyMAMPS brushes-coated surfaces with a brush thickness of (e) ~8 nm, (f) ~16 nm, (g) ~25 nm, (h) ~34 nm, and (i) ~42 nm. Error bars in (b) and (c) represent the standard deviation of the mean (n = 3).

Surface roughness is another key factor to affect antifouling performance. Rough brushes, despite their intrinsic antifouling capacity, can still kinetically trap the approaching proteins on their heterogeneous valleys. Visual inspection of tapping-mode AFM images in Fig. 3d-i showed that as a control, initiator-coated Au surface was very smooth, with a root-mean-square (RMS) roughness value of 0.045 nm. PolyMAMPS brush with ~8 nm thickness was largely covered by many small, isolated clusters, resulting in a RMS roughness value of 1.89 nm. As brush thickness increased from ~8 to ~25 nm, polyMAMPS brush became denser and smoother, leading to a decreased surface roughness from ~1.89 nm to ~0.32 nm. However, further increase of brush thickness to ~34 nm and ~42 nm resulted in a slight increase of surface roughness to ~0.72 and ~0.92 nm, respectively. As presented above, while too low or too high brush thicknesses appear to increase surface roughness to some extents, the SI-ATRP process enables to efficiently graft polymer chains with high packing density and surface uniformity on Au substrates in a wide range of thickness.

3.2. Surface resistance of polyMAMPS brushes to proteins

Our previous antifouling studies have revealed an optimal range of brush thickness of ~20 to 40 nm, in which polyacrylamide brushes (polyHEMA, polyHPMA, polyHEAA, polyAAEE and polyNAGA) and polyzwitterion brushes (polySVBA and polyVBIPS) can achieve superlow fouling (<5 ng·cm^{-2}) or nonfouling (<0.3 ng·cm^{-2}) of protein adsorption.[16,22,34,35,37,46] Therefore, as a proof-of-concept, polyMAMPS brushes of ~25 nm were first prepared and tested for their protein adsorption/resistance capacity from both undiluted (100%) blood plasma and serum at room temperature using SPR. As shown in Fig. 4a, typical SPR sensorgrams showed that upon flowing undiluted blood serum and plasma through independent SPR channels coated with polyMAMPS brushes (~25 nm film thickness), a large amount of proteins of ~796 ng·cm^{-2} from blood plasma and ~470 ng·cm^{-2} from blood serum was adsorbed immediately on polyMAMPS brushes. However, when switching from protein solution to PBS solution, these initially adsorbed proteins were immediately and almost completely removed from the polyMAMPS brushes, leading to a final amount of adsorbed proteins of ~1.4 ng·cm^{-2} (plasma) and ~4.0 ng·cm^{-2} (serum) at a superlow fouling level (<5 ng·cm^{-2}). This indicates that initially adsorbed proteins were very loosely bound to polyMAMPS brushes and thus can be easily washed away by any external flow.

Further, we studied the effect of brush thickness on protein adsorption from undiluted blood plasma and serum. In Fig. 4b, a very thin polyMAMPS brush of < 6 nm led to a large amount of adsorbed proteins from blood plasma (~88 ng·cm^{-2}). As brush thickness was increased to a range of ~20–34 nm, polyMAMPS brushes achieved a stable plateau of adsorbed proteins at an ultralow fouling level of ~1.5 ng·cm^{-2}. However, further increase of brush thickness to 40–54 nm led to a large increase in protein adsorption of ~5–70 ng·cm^{-2} again. Similarly, Fig. 4c showed the similar thickness dependence of polyMAMPS brushes on protein adsorption from undiluted human blood serum. Except for a very thin brush to induce a large amount of protein adsorption (~58 ng·cm^{-2}), polyMAMPS brushes with a thickness range of 25–34 nm enabled to effectively prevent protein adsorption from blood serum and retain at an ultralow fouling level of ~1.4 ng·cm^{-2}. It appears that serum proteins are more effectively prevented to be adsorbed on polyMAMPS brushes than plasma proteins, presumably due to the absence of anticoagulants of EDTA or heparin [53]. Taken together, polyMAMPS brush with ~25 nm thickness exhibited the higher surface hydrophilicity (i.e. water contact angle=~32°), the smaller surface roughness (i.e. RMS = 0.32 nm), and the lower protein adsorption (i.e. ~1.4 ng·cm^{-2} from plasma and ~4.0 ng·cm^{-2} from serum). In our cases, for a given surface with the same surface chemistry, while we observed that polyMAMPS brushes exhibited the lower fouling behavior as surface roughness decreased from ~1.89 nm to ~0.32 nm, we should also notice that the relatively larger surface roughness occurred at the thicker film thickness (i.e. longer chains), in which the longer chains have stronger steric repulsion to prevent foulant adsorption [54,55]. Thus, the competition between surface roughness and chain length may account for antifouling property of polymer brushes with the same grafting density. Moreover, large surface roughness not only increases a possibility to kinetically trap the foulants (i.e. increase of fouling from a kinetic viewpoint), but also decreases the entropy change of water molecules before and after binding to surfaces (i.e. free energy of foulant adsorption becomes more favorable), thus both effects increase the fouling of polymer brushes.

3.3. Cell adhesion on polyMAMPS brushes

Considering that one of major antifouling applications is to interact with adhesive cells *in vivo* or *in vitro* for implants, drug/gene delivery carriers, and wound dressings, here we study the resistance of polyMAMPS brushes with different thicknesses to the adhesion of bovine aortic endothelial cells (BAECs) that is directly related to surface-induced thrombosis and hemocompatibility. After 3-day co-culture of cells in the presence of different surfaces at 37 °C, initiator-coated surface as a control was entirely covered by BAEC as expected, with the adhered cell density of ~8.51 × 10^4 cells·cm^{-2} (Fig. 5a) In sharp contrast, polyMAMPS brushes of 8–34 nm thickness significantly reduced cell adhesion. Visual inspection showed that some scattered cells were still adhered on the thin polyMAMPS brushes of ~8 nm thickness (Fig. 5b), with

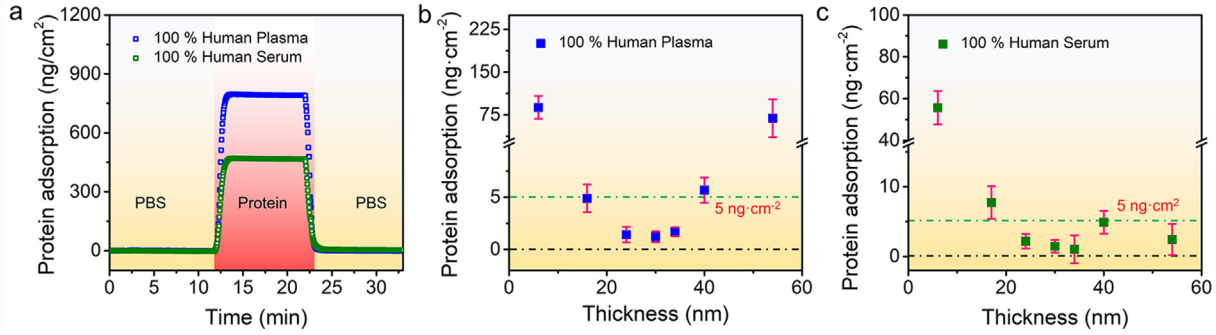

Fig. 4. (a) Typical SPR sensorgrams to show protein adsorption from both undiluted human blood serum and plasma on polyMAMPS brush of ~25 nm thickness. Dependence of protein adsorption from undiluted human blood (b) plasma and (c) serum on polyMAMPS brushes with different brush thicknesses of 8–54 nm.

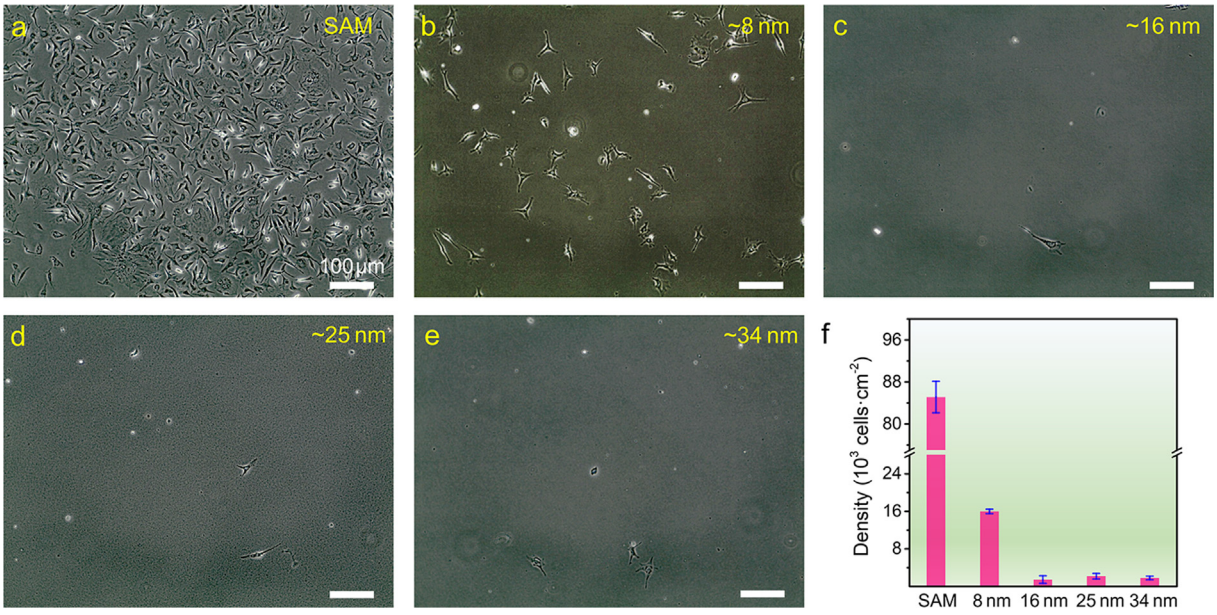

Fig. 5. Representative microscopy images of BAEC attachment on (a) initiator-coated surface and polyMAMPS brushes with different brush thickness of (b) ~8 nm, (c) ~16 nm, (d) ~25 nm, and (e) ~34 nm after 3-day cell culture at 37 °C. (f) Statistical analysis of the adhered BAEC cell density on the abovementioned surfaces (n = 3).

non-negligible adhered cell density of ~1.59 × 10^5 cells·cm^{-2}. However, as the brush thickness increased to 16, 25, and 34 nm (Fig. 5c-e), there were almost no adhered cells being observed on these three polyMAMPS brushes, and the adhered cell density remained at the similar level of ~1.72 × 10^4 cells·cm^{-2}. The cell adhesion results confirm that polyMAMPS brushes of >16 nm thickness achieve high surface resistance to BAEC adhesion, consistent with the inhibition of protein adsorption on polyMAMPS brushes with the higher thicknesses.

3.4. Bacterial attachment on polyMAMPS brushes

On the basis of the excellent resistance of polyMAMPS brushes against protein adsorption and cell adhesion, we continued to challenge polyMAMPS brushes with two typical bacterial strains of Gram-negative *E. coli* and Gram-positive *S. epidermidis*. Both strains are often associated with pneumonia, and urinary tract, surgical site, and bloodstream infections. In brief, several colonies of each bacteria were firstly selected and incubated in moderate LB medium to obtain the initial bacterial culture solutions. Next, the initial bacterial solutions were diluted to achieve a final density of ~10^5 cells/cm^2. A diluted 4 mL bacterial suspension was then added to each well after the sterilized chips grafted with polyMAMPS brushes of various thicknesses were placed into a six-well flask at the room temperature for ~12 h. Finally, all surfaces were rinsed with Milli-Q water and only the surface-attached bacterial cells were counted. As a control, *E. coli* proliferated and spread on the initiator-coated surface (Fig. 6a) and attained almost full coverage of ~1.92 × 10^6 cells·cm^{-2} after initial cell seeding (Fig. 6f). In contrast, polyMAMPS brushes of different thicknesses were found to have strong surface resistance to *E. coli* attachment. While thin polyMAMPS brush of ~8 nm thickness showed ~2.46 × 10^5 cells·cm^{-2} of adsorbed *E. coli*, which is an approximate 86% reduction in *E. coli* adhesion as compared to the control, the other three polyMAMPS brushes only exhibited very few bacteria cells, as evidenced by ~2.35 × 10^4, ~2.09 × 10^4, and ~1.57 × 10^4 cells·cm^{-2} (Fig. 6b-e), indicating a 87–92% reduction in the number of bacterial adhered on initiator-coated surface. Similarly, polyMAMPS brushes also showed high surface resistance to *S. epidermidis* attachment (Fig. 7a-e). The adhered *S. epidermidis* on polyMAMPS brushes of ~8–34 nm were ~8.37 × 10^4, ~3.14 × 10^4, ~1.31 × 10^4, and ~0.52 × 10^4 cells·cm^{-2}, respectively (Fig. 7f). PolyMAMPS brushes appear to be more effective to resist *E. coli* than *S. epidermidis*, due to the electrostatic interaction between a large amount of exposed sulfonic acid groups in polyzwitterion brushes and the charged matrixes of bacteria, i.e. electrostatic repulsion for *E. coli* and electrostatic attraction for *S. epidermidis*. We also summarized and compared typical and well-studied antifouling polymer brushes for surface resistance to non-specific proteins from undiluted human blood plasma and serum, as well as cell/bacteria adhesion (Table S1).

3.5. Protein resistance to Agar/PolyMAMPS DN hydrogel

Upon demonstrating excellent antifouling performance of polyMAMPS brushes as a model system containing micro-scale structure, we designed and synthesized a new class of Agar/polyMAMPS hydrogels with a double-network (DN) structure, consisting of polysaccharide-based agarose (Agar) as the first physical network and zwitterionic polyMAMPS as the second chemical network. We have developed a number of Agar-based DN hydrogels, including Agar/PAAm [56], Agar/PHEAA [57], Agar/PAAc/Fe^{3+} [58], and Agar/PAAEE [59], all of which exhibited superior mechanical properties (e.g. tensile stress of 0.32–2.6 MPa, tensile strain of 250%-2000%, fracture energy of 1520–1620 kJ m^{-3}, stiffness/toughness recovery of 60%-100%/30%-100%). Among them, Agar/PAAm hydrogels demonstrated their antifouling properties against protein adsorption. In this work, considering that Agar (polysaccharide materials) are well-known fouling materials and often used as growth medium to culture bacteria and cells, we aim to demonstrate that the integration of zwitterionic antifouling polyMAMPS network into fouling Agar network can still retain overall antifouling property of Agar/polyMAMPS hydrogels. FT-IR spectra in Fig. S2 characterized the chemical structure variation of typical Agar SN and Agar/polyMAMPS DN hydrogels. It is clearly shown that a distinct characteristic peak appears at ~990 cm^{-1} corresponding to the bending vibration of –S═O from sulfonate residues of polyMAMPS chains. Fig. 8a showed the adsorption ratio of fibrinogen

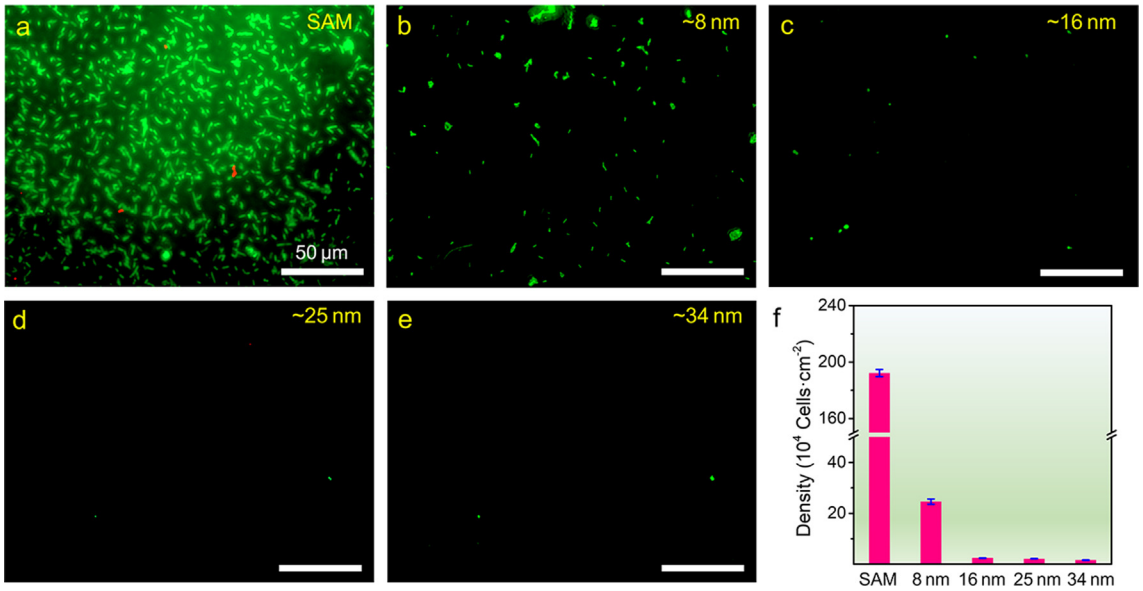

Fig. 6. Representative confocal microscopy of *E. coli* attachment on (a) initiator-coated surface and polyMAMPS brushes with different thicknesses of (b) ~8 nm, (c) ~16 nm, (d) ~25 nm, and (e) ~34 nm after 12 h incubation. (f) Statistical analysis of adhered *E. coli* density on different surfaces (n = 3).

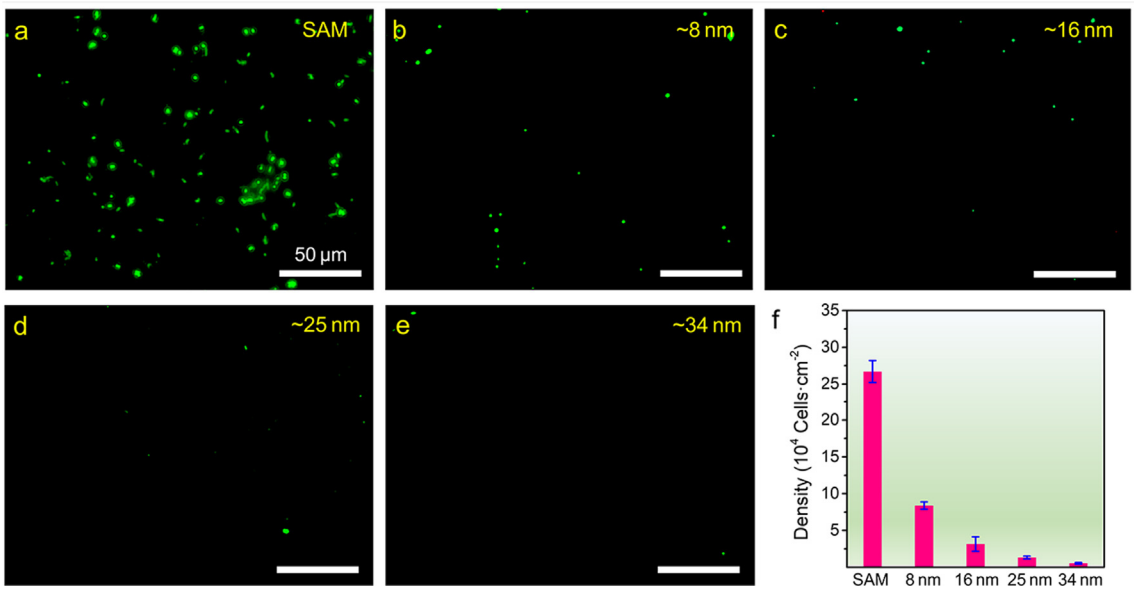

Fig. 7. Representative confocal microscopy of *S. epidermidis* attachment on (a) initiator-coated surface and polyMAMPS brushes with different thicknesses of (b) ~8 nm, (c) ~16 nm, (d) ~25 nm, and (e) ~34 nm after 12 h incubation. (f) Statistical analysis of adhered *S. epidermidis* density on different surfaces (n = 3).

(Fg) onto Agar/polyMAMPS DN gels and their respective SN gels, as measured by ELISA. The adsorption ratio is defined by Fg_{Gel}/Fg_{TCPS}, where surface of tissue culture polystyrene (TCPS) was used as a control for comparison. There was no surprise to observe that Agar SN gels (~30 g·L^{-1}) can adsorb ~43% of Fg adsorption relative to TCPS, while polyMAMPS SN gels can still retain its antifouling properties against Fg adsorption (~4%) relative to TCPS, demonstrating that polyMAMPS polymer chains effectively resisted Fg protein adsorption. More interestingly, upon the combination of fouling Agar network and antifouling polyMAMPS network, Agar/polyMAMPS DN hydrogels still exhibited superb surface resistance to Fg adsorption of ~8%. It is likely that both interpenetrating DN networks consume their strong interactions with each other and with surrounding water molecules, thus reducing their potential interactions with proteins. This hypothesis can be further supported by the comparison of Fg adsorption on Agar/polyMAMPS DN hydrogels with and without MBAA crosslinkers. Crosslinked Agar/polyMAMPS hydrogels (8%) adsorbed less Fg than non-crosslinked ones (20%), indicating that crosslinked networks further promoted network-network and network-water interactions within the hydrogels at the expense of reduction in their interactions with external proteins, thus leading to the better antifouling property. Similar results of surface resistance to bacteria attachment for these four hydrogels were provided in Fig. 8b. The statistical values of adhered bacteria density were summarized in Figs. S3 and S4. It is clearly shown that the adhered density of *E. coli*/*S. epidermidis* are ~2.62 × 10^5/~2.10 × 10^5, ~1.83 × 10^4/~2.36 × 10^4, ~4.45 × 10^4/~3.40 × 10^4, and ~1.23 × 10^4/~7.33 × 10^4 cells·cm^{-2} for Agar SN, polyMAMPS SN, Agar/polyMAMPS DN hydrogels with and without MBAA crosslinkers, respectively.

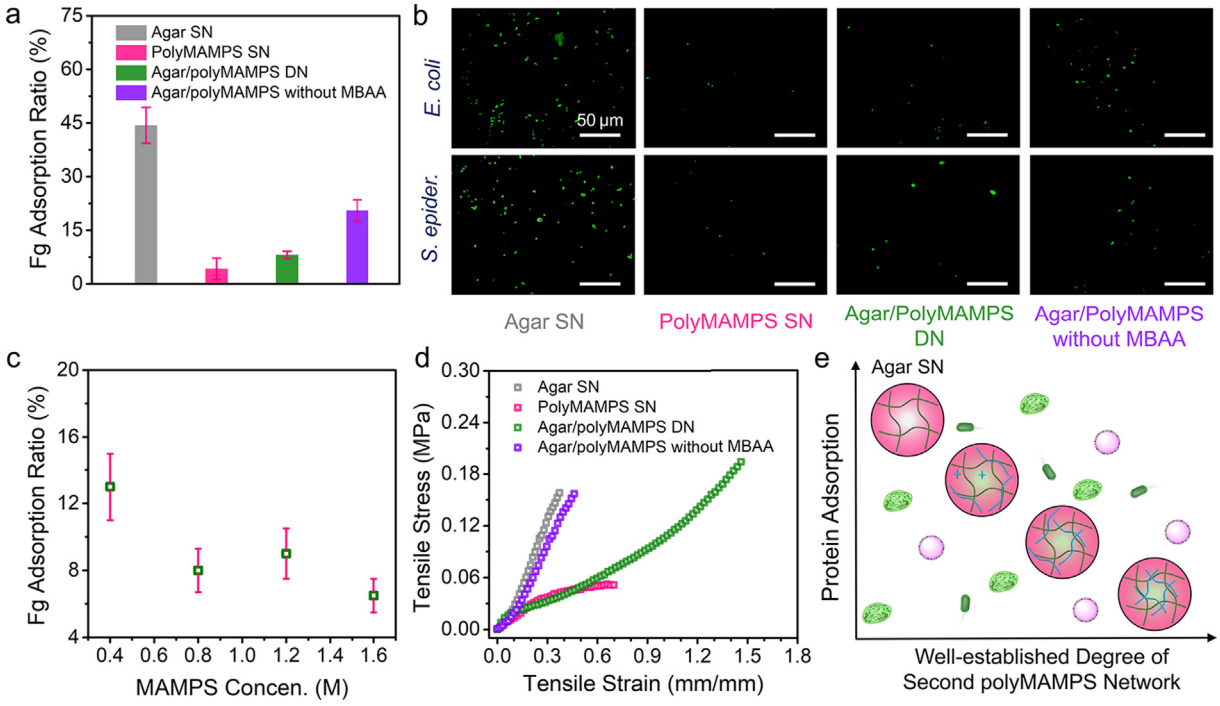

Fig. 8. Antifouling and mechanical properties of polyMAMPS-based hydrogels. (a) Fibrinogen adsorption and (b) Bacteria adhesion (*E. coli* and *S. epider.*) onto Agar SN, polyMAMPS SN, Agar/polyMAMPS DN hydrogels with and without MBAA crosslinkers. (c) Effect of MAMPS concentrations on fibrinogen adsorption of Agar/polyMAMPS DN hydrogels. (d) Tensile stress-strain curves of Agar SN, polyMAMPS SN, and Agar/polyMAMPS DN hydrogels with and without MBAA crosslinkers. (e) A mechanical property-protein adsorption correlation for polyMAMPS-based hydrogels.

To better understand how zwitterionic network works, we further examined the concentration effect of MAMPS on the antifouling property of Agar/polyMAMPS DN hydrogels. We synthesized a series of Agar/polyMAMPS DN hydrogels by varying the MAMPS concentrations of 0.4–1.6 M and fixing Agar concentration of ~30 g·L^{-1}. As shown in Fig. 8c, the increase of zwitterionic MAMPS monomer concentration from 0.4 M to 1.6 M led to the increased chain length and amount of polyMAMPS network, and both effects caused the reduction of Fg adsorption from ~13% to ~6%, as compared with TCPS. To better understand the mechanical role of the second polyMAMPS network in antifouling property of Agar/polyMAMPS hydrogels, we prepared Agar SN, polyMAMPS SN, and Agar/polyMAMPS DN hydrogels with and without MBAA crosslinkers, tested their tensile properties, and then correlated mechanical properties with antifouling performance. As shown in Fig. 8d, both Agar and polyMAMPS gels with single-network structures exhibited very weak and brittle character, as evidenced by the tensile strain of ~0.16 MPa at ~40% strain and ~0.052 MPa at ~72% strain, respectively. Similarly, without assistance of MBAA crosslinker, the introduction of polyMAMPS into Agar network did not significantly improve the tensile properties of Agar/polyMAMPS DN hydrogels, with weak tensile stress of ~0.16 MPa at ~45% strain, almost similar to that of Agar SN gel. In sharp contrast, upon crosslinking the second polyMAMPS network that interpenetrates with the agar network, the resultant Agar/polyMAMPS DN hydrogels largely improved their tensile stress to 0.21 MPa and tensile strain to 145%, showing 0.21/0.16-time higher than those of agar SN gel, 0.21/0.05-time higher than those of polyMAMPS SN gel, and 0.21/0.16-time higher than those of Agar/polyMAMPS DN gel without MBAA. Comparison of antifouling performance and mechanical properties between these hydrogels revealed a correlation that tough hydrogels exhibited the better antifouling property (Fig. 8e), presumably because the strong intra- and inter-interactions between polymeric chains in the hydrogel would consume all possible interactive sites, making hydrogels difficult or infeasible to interact with proteins.

4. Conclusions

We have designed and synthesized a new zwitterionic monomer (MAMPS) and then fabricated these monomers into polyMAMPS polymers, which were grafted on Au substrate to form polyMAMPS brushes by SI-ATRP and interpenetrated with Agar network to form Agar/polyMAMPS DN hydrogels by heating–cooling-UV polymerization. First, polyMAMPS brushes with optimal thickness of 20–40 nm and high grafting density exhibited high surface resistance to non-specific protein adsorption (0.3–5 ng/cm^2) from resisting undiluted human blood serum/plasma, cell adhesion (<10^4 cells·cm^{-2}), and bacteria attachment (<10^5 cells/cm^2) up to 72 h. Then, Agar/polyMAMPS DN hydrogels with high tensile stress of 0.21 MPa and tensile strain of 145% significantly reduced protein adhesion and bacteria attachment, as compared to Agar SN hydrogels, demonstrating that introduction of antifouling polyMAMPS network into fouling Agar network can effectively consume interactive fouling sites of Agar network by polyMAMPS-Agar interactions, which in turn competitively reduce gel-protein interactions, leading to the better antifouling property of DN hydrogels. This work demonstrates the intrinsic antifouling property of polyMAMPS at both microscopic and macroscopic length scales and highlights the importance of surface hydration in antifouling property, which hopefully will guide the structural-based design of new zwitterionic materials beyond traditional polyCBMA, polySBMA, and polyMPC materials. In a broader view, the development of a wide variety of antifouling materials with different chemical structures can not only overcome the material-depended fouling-resistance issue of foulants by nature selection, but also promote interdisciplinary research from fundamental design, characterization, and modification of

antifouling materials to practical applications of these materials at microscopic and macroscopic scales. Furthermore, the use of data-driven artificial intelligent materials design is another promising research direction for developing next-generation antifouling materials and deriving the fundamental structure-property relationship of antifouling materials.

CRediT authorship contribution statement

Dong Zhang: Methodology, Investigation, Writing - original draft. **Baiping Ren:** Investigation, Writing - review & editing. **Yanxian Zhang:** Investigation, Writing - review & editing. **Yonglan Liu:** Investigation, Writing - review & editing. **Hong Chen:** Investigation, Writing - review & editing. **Shengwei Xiao:** Investigation, Writing - review & editing. **Yung Chang:** Methodology, Writing - review & editing. **Jintao Yang:** Methodology, Writing - review & editing. **Jie Zheng:** Methodology, Writing - original draft, Supervision, Writing - review & editing.

Declaration of Competing Interest

The authors declare that they have no known competing financial interests or personal relationships that could have appeared to influence the work reported in this paper.

Acknowledgment

J. Z. thanks financial supports from NSF (DMR-1806138 and CMMI-1825122). We also thank Louisa Wang from Hathaway Brown School for her hard work in our lab.

Appendix A. Supplementary data

Supplementary data to this article can be found online at https://doi.org/10.1016/j.jcis.2020.05.122.

References

[1] H. Liu, L. Liu, X. Jiang, J. Fan, W. Peng, P. Liu, T. Yang, H. Chen, W. Jiang, G. Yin, P. Liu, J. Shen, Rational design of a zwitterionic–phosphonic copolymer for the surface antifouling modification of multiple biomedical metals, J. Mater. Chem. B 7 (25) (2019) 4055–4065.
[2] Q. Zeng, Y. Zhu, B. Yu, Y. Sun, X. Ding, C. Xu, Y.W. Wu, Z. Tang, F.J. Xu, Antimicrobial and antifouling polymeric agents for surface functionalization of medical implants, Biomacromolecules 19 (7) (2018) 2805–2811.
[3] T. Huang, H. Liu, P. Liu, P. Liu, L. Li, J. Shen, Zwitterionic copolymers bearing phosphonate or phosphonic motifs as novel metal-anchorable anti-fouling coatings, J. Mater. Chem. B 5 (27) (2017) 5380–5389.
[4] Y. Wang, L. Wang, B. Li, Y. Cheng, D. Zhou, X. Chen, X. Jing, Y. Huang, Compact vesicles self-assembled from binary graft copolymers with high hydrophilic fraction for potential drug/protein delivery, ACS Macro Lett. 6 (11) (2017) 1186–1190.
[5] H. Wang, F. Cheng, W. Shen, G. Cheng, J. Zhao, W. Peng, J. Qu, Amino acid-based anti-fouling functionalization of silica nanoparticles using divinyl sulfone, Acta Biomater. 40 (2016) 273–281.
[6] R. Ciriminna, F.V. Bright, M. Pagliaro, Ecofriendly antifouling marine coatings, ACS Sustainable Chem. Eng. 3 (4) (2015) 559–565.
[7] A.G. Nurioglu, A.C.C. Esteves, G. de With, Non-toxic, non-biocide-release antifouling coatings based on molecular structure design for marine applications, J. Mater. Chem. B 3 (32) (2015) 6547–6570.
[8] A.L. Patterson, B. Wenning, G. Rizis, D.R. Calabrese, J.A. Finlay, S.C. Franco, R.N. Zuckermann, A.S. Clare, E.J. Kramer, C.K. Ober, R.A. Segalman, Role of backbone chemistry and monomer sequence in amphiphilic oligopeptide- and oligopeptoid-functionalized PDMS- and PEO-based block copolymers for marine antifouling and fouling release coatings, Macromolecules 50 (7) (2017) 2656–2667.
[9] C.S. Ware, T. Smith-Palmer, S. Peppou-Chapman, L.R.J. Scarratt, E.M. Humphries, D. Balzer, C. Neto, Marine antifouling behavior of lubricant-infused nanowrinkled polymeric surfaces, ACS Appl. Mater. Interfaces 10 (4) (2018) 4173–4182.
[10] P. Zhang, P. Jain, C. Tsao, Z. Yuan, W. Li, B. Li, K. Wu, H.C. Hung, X. Lin, S. Jiang, Polypeptides with high zwitterion density for safe and effective therapeutics, Angew. Chem. Int. Ed. Engl. 57 (26) (2018) 7743–7747.
[11] C. Leng, S. Sun, K. Zhang, S. Jiang, Z. Chen, Molecular level studies on interfacial hydration of zwitterionic and other antifouling polymers in situ, Acta Biomater. 40 (2016) 6–15.
[12] R. Zhang, Y. Liu, M. He, Y. Su, X. Zhao, M. Elimelech, Z. Jiang, Antifouling membranes for sustainable water purification: strategies and mechanisms, Chem. Soc. Rev. 45 (21) (2016) 5888–5924.
[13] D. Rana, T. Matsuura, Surface modifications for antifouling membranes, Chem. Rev. 110 (4) (2010) 2448–2471.
[14] Y. Higaki, M. Kobayashi, D. Murakami, A. Takahara, Anti-fouling behavior of polymer brush immobilized surfaces, Polym. J. 48 (4) (2016) 325–331.
[15] X. Shi, X. Zhu, Biofilm formation and food safety in food industries, Trends Food Sci. Technol. 20 (9) (2009) 407–413.
[16] F. Yang, Y. Liu, Y. Zhang, B. Ren, J. Xu, J. Zheng, Synthesis and characterization of ultralow fouling poly(N-acryloyl-glycinamide) brushes, Langmuir 33 (49) (2017) 13964–13972.
[17] L. Zeng, Y. Wu, J.-F. Xu, S. Wang, X. Zhang, Supramolecular switching surface for antifouling and bactericidal activities, ACS Appl. Bio Mater. 2 (2) (2019) 638–643.
[18] S.B. Darling, Perspective: Interfacial materials at the interface of energy and water, J. Appl. Phys. 124 (3) (2018) 030901.
[19] R.G. Nuzzo, Stable antifouling surfaces, Nat. Mater. 2 (4) (2003) 207.
[20] Y. Yonehara, H. Yamashita, C. Kawamura, K. Itoh, A new antifouling paint based on a zinc acrylate copolymer, Prog. Org. Coat. 42 (2001) 150–158.
[21] Y. Tang, X. Cai, Y. Xiang, Y. Zhao, X. Zhang, Z. Wu, Cross-linked antifouling polysaccharide hydrogel coating as extracellular matrix mimics for wound healing, J. Mater. Chem. B 5 (16) (2017) 2989–2999.
[22] H. Chen, M. Zhang, J. Yang, C. Zhao, R. Hu, Q. Chen, Y. Chang, J. Zheng, Synthesis and characterization of antifouling poly(N-acryloylaminoethoxyethanol) with ultralow protein adsorption and cell attachment, Langmuir 30 (34) (2014) 10398–10409.
[23] F. Sun, H.C. Hung, A. Sinclair, P. Zhang, T. Bai, D.D. Galvan, P. Jain, B. Li, S. Jiang, Q. Yu, Hierarchical zwitterionic modification of a SERS substrate enables real-time drug monitoring in blood plasma, Nat. Commun. 7 (2016) 13437.
[24] L. Xie, F. Hong, C. He, C. Ma, J. Liu, G. Zhang, C. Wu, Coatings with a self-generating hydrogel surface for antifouling, Polymer 52 (17) (2011) 3738–3744.
[25] C. Cheng, A. He, C. Nie, Y. Xia, C. He, L. Ma, C. Zhao, One-pot cross-linked copolymerization for the construction of robust antifouling and antibacterial composite membranes, J. Mater. Chem. B 3 (20) (2015) 4170–4180.
[26] L. Huang, L. Zhang, S. Xiao, Y. Yang, F. Chen, P. Fan, Z. Zhao, M. Zhong, J. Yang, Bacteria killing and release of salt-responsive, regenerative, double-layered polyzwitterionic brushes, Chem. Eng. J. 333 (2018) 1–10.
[27] R. Bai, Q. Zhang, L. Li, P. Li, Y.J. Wang, O. Simalou, Y. Zhang, G. Gao, A. Dong, N-halamine-containing electrospun fibers kill bacteria via a contact/release co-determined antibacterial pathway, ACS Appl. Mater. Interfaces 8 (46) (2016) 31530–31540.
[28] Y. Wang, J. Wu, D. Zhang, F. Chen, P. Fan, M. Zhong, S. Xiao, Y. Chang, X. Gong, J. Yang, J. Zheng, Design of salt-responsive and regenerative antibacterial polymer brushes with integrated bacterial resistance, killing, and release properties, J. Mater. Chem. B 7 (38) (2019) 5762–5774.
[29] J. Wu, D. Zhang, Y. Wang, S. Mao, S. Xiao, F. Chen, P. Fan, M. Zhong, J. Tan, J. Yang, Electric assisted salt-responsive bacterial killing and release of polyzwitterionic brushes in low-concentration salt solution, Langmuir 35 (25) (2019) 8285–8293.
[30] X. Zhang, Y. Shu, S. Su, J. Zhu, One-step coagulation to construct durable anti-fouling and antibacterial cellulose film exploiting Ag@AgCl nanoparticle-triggered photo-catalytic degradation, Carbohydr. Polym. 181 (2018) 499–505.
[31] X. Zhang, J. Zhang, J. Yu, Y. Zhang, F. Yu, L. Jia, Y. Tan, Y. Zhu, B. Hou, Enhancement in the photocatalytic antifouling efficiency over cherimoya-like InVO4/BiVO4 with a new vanadium source, J. Colloid Interface Sci. 533 (2019) 358–368.
[32] S. Andjouh, Y. Blache, Screening of bromotyramine analogues as antifouling compounds against marine bacteria, Biofouling 32 (8) (2016) 871–881.
[33] H. Chen, Q. Chen, R. Hu, H. Wang, B.-m.Z. Newby, Y. Chang, J. Zheng, Mechanically strong hybrid double network hydrogels with antifouling properties, J. Mater. Chem. B 3 (27) (2015) 5426–5435.
[34] H. Chen, C. Zhao, M. Zhang, Q. Chen, J. Ma, J. Zheng, Molecular understanding and structural-based design of polyacrylamides and polyacrylates as antifouling materials, Langmuir 32 (14) (2016) 3315–3330.
[35] C. Zhao, J. Zheng, Synthesis and characterization of poly(N-hydroxyethylacrylamide) for long-term antifouling ability, Biomacromolecules 12 (11) (2011) 4071–4079.
[36] J. Yang, M. Zhang, H. Chen, Y. Chang, Z. Chen, J. Zheng, Probing the structural dependence of carbon space lengths of poly(N-hydroxyalkyl acrylamide)-based brushes on antifouling performance, Biomacromolecules 15 (8) (2014) 2982–2991.
[37] C. Zhao, L. Li, Q. Wang, Q. Yu, J. Zheng, Effect of film thickness on the antifouling performance of poly(hydroxy-functional methacrylates) grafted surfaces, Langmuir 27 (8) (2011) 4906–4913.
[38] S.Y. Jiang, Z.Q. Cao, Ultralow-fouling, functionalizable, and hydrolyzable zwitterionic materials and their derivatives for biological applications, Adv. Mater. 22 (9) (2010) 920–932.
[39] J.B. Schlenoff, Zwitteration: coating surfaces with zwitterionic functionality to reduce nonspecific adsorption, Langmuir 30 (32) (2014) 9625–9636.
[40] Q. Shao, S. Jiang, Molecular understanding and design of zwitterionic materials, Adv. Mater. 27 (1) (2015) 15–26.

[41] Z. Zhang, T. Chao, S. Chen, S. Jiang, Superlow fouling sulfobetaine and carboxybetaine polymers on glass slides, Langmuir 22 (24) (2006) 10072–10077.
[42] G. Cheng, H. Xue, Z. Zhang, S. Chen, S. Jiang, A switchable biocompatible polymer surface with self-sterilizing and nonfouling capabilities, Angew. Chem. Int. Ed. Engl. 47 (46) (2008) 8831–8834.
[43] N. Sun, M. Liu, J. Wang, Z. Wang, X. Li, B. Jiang, R. Pei, Chitosan nanofibers for specific capture and nondestructive release of CTCs assisted by pCBMA brushes, Small 12 (36) (2016) 5090–5097.
[44] G. Cheng, G. Li, H. Xue, S. Chen, J.D. Bryers, S. Jiang, Zwitterionic carboxybetaine polymer surfaces and their resistance to long-term biofilm formation, Biomaterials 30 (28) (2009) 5234–5240.
[45] J. Wu, D. Zhang, L. Zhang, B. Wu, S. Xiao, F. Chen, P. Fan, M. Zhong, J. Tan, Y. Chu, J. Yang, Long-term stability and salt-responsive behavior of polyzwitterionic brushes with cross-linked structure, Prog. Org. Coat. 134 (2019) 153–161.
[46] D. Zhang, Y. Fu, L. Huang, Y. Zhang, B. Ren, M. Zhong, J. Yang, J. Zheng, Integration of antifouling and antibacterial properties in salt-responsive hydrogels with surface regeneration capacity, J. Mater. Chem. B 6 (6) (2018) 950–960.
[47] S. Xiao, Y. Zhang, M. Shen, F. Chen, P. Fan, M. Zhong, B. Ren, J. Yang, J. Zheng, Structural dependence of salt-responsive polyzwitterionic brushes with an anti-polyelectrolyte effect, Langmuir 34 (1) (2018) 97–105.
[48] H. Chen, J. Yang, S. Xiao, R. Hu, S.M. Bhaway, B.D. Vogt, M. Zhang, Q. Chen, J. Ma, Y. Chang, L. Li, J. Zheng, Salt-responsive polyzwitterionic materials for surface regeneration between switchable fouling and antifouling properties, Acta Biomater. 40 (2016) 62–69.
[49] A. Laschewsky, Structures and synthesis of zwitterionic polymers, Polymers 6 (5) (2014) 1544–1601.
[50] E. van Andel, S.C. Lange, S.P. Pujari, E.J. Tijhaar, M.M.J. Smulders, H.F.J. Savelkoul, H. Zuilhof, Systematic comparison of zwitterionic and non-zwitterionic antifouling polymer brushes on a bead-based platform, Langmuir 35 (5) (2019) 1181–1191.
[51] J. Zhu, M. Tian, J. Hou, J. Wang, J. Lin, Y. Zhang, J. Liu, B. Van der Bruggen, Surface zwitterionic functionalized graphene oxide for a novel loose nanofiltration membrane, J. Mater. Chem. A 4 (5) (2016) 1980–1990.
[52] V. Yesilyurt, O. Veiseh, J.C. Doloff, J. Li, S. Bose, X. Xie, A.R. Bader, M. Chen, M.J. Webber, A.J. Vegas, R. Langer, D.G. Anderson, A facile and versatile method to endow biomaterial devices with zwitterionic surface coatings, Adv Healthc Mater 6 (4) (2017).
[53] V.L. Stevens, E. Hoover, Y. Wang, K.A. Zanetti, Pre-analytical factors that affect metabolite stability in human urine, plasma, and serum: a review, Metabolites 9 (8) (2019).
[54] S.I. Jeon, J.D. Andrade, Protein surface interactions in the presence of polyethylene oxide. 2. Effect of protein size, J Colloid Interf Sci 142 (1) (1991) 159–166.
[55] T. McPherson, A. Kidane, I. Szleifer, K. Park, Prevention of protein adsorption by tethered poly(ethylene oxide) layers: experiments and single-chain mean-field analysis, Langmuir 14 (1) (1998) 176–186.
[56] Q. Chen, L. Zhu, C. Zhao, Q. Wang, J. Zheng, A robust, one-pot synthesis of highly mechanical and recoverable double network hydrogels using thermoreversible sol-gel polysaccharide, Adv. Mater. 25 (30) (2013) 4171–4176.
[57] H. Chen, Y. Liu, B. Ren, Y. Zhang, J. Ma, L. Xu, Q. Chen, J. Zheng, Super bulk and interfacial toughness of physically crosslinked double-network hydrogels, Adv. Funct. Mater. 27 (44) (2017) 1703086.
[58] X. Li, Q. Yang, Y. Zhao, S. Long, J. Zheng, Dual physically crosslinked double network hydrogels with high toughness and self-healing properties, Soft Matter 13 (5) (2017) 911–920.
[59] Y. Zhang, B. Ren, S. Xie, Y. Cai, T. Wang, Z. Feng, J. Tang, Q. Chen, J. Xu, L. Xu, J. Zheng, Multiple physical cross-linker strategy to achieve mechanically tough and reversible properties of double-network hydrogels in bulk and on surfaces, ACS Appl. Polym. Mater. 1 (4) (2019) 701–713.